ACI's Special Publication for the Fourth International Symposium on Fiber Reinforced Polymer for Reinforced Concrete Structures (FRPRCS-4), 1999.

Modeling the Stress State Dependency of the Bond Behavior of FRP Tendons

James V. Cox and Jun Guo

Synopsis: The bond behavior of carbon FRP tendons for concrete is characterized with an interface model. In particular tendons with a surface structure that produce significant mechanical interlocking with the adjacent concrete are considered. This type of mechanical interaction can produce damage in the adjacent concrete and within the surface structure of the reinforcing element. The combination of these mechanisms is characterized with an elastoplasticity model that fully couples the longitudinal and radial response; the model calibration is based upon a series of bond tests under differing stress states. The model does not provide a detailed description of the underlying mechanics associated with the progressive bond failure, and it will generally require recalibration when applied to significantly different FRP bars or tendons. However, using a calibration for a GFRP bar, the model gives acceptable estimates of the bond strength for several tests of a particular CFRP tendon, even though the specimens have significantly different attributes. Additional validation tests (using data with measures of the experimental scatter) are needed to define the predictive limits of the model; nonetheless the transfer length problem further demonstrates the potential application of the model to help predict and understand the behavior of FRP-reinforced structural components.

ACI's Special Publication for the Fourth International Symposium on Fiber Reinforced Polymer for Reinforced Concrete Structures (FRPRCS-4), 1999.

James V. Cox is an assistant professor of civil engineering at Johns Hopkins University, Baltimore, MD. His research interests are in modeling of reinforced concrete, composite materials, constitutive modeling, and computational mechanics. His recent work has focused on characterizing (at two different scales) the mechanical interaction between both steel and FRP bars and concrete.

Jun Guo is a Ph.D. student in the civil engineering department at Johns Hopkins University. His research focuses on numerical modeling of the mechanical interaction between FRP reinforcing bars and tendons with concrete.

INTRODUCTION

The need for infrastructure renewal and the potential advantages of composite materials (*e.g.*, improved life cycle costs) has led to increased interest in applying composite materials to civil engineering structures. One application is to use fiber-reinforced polymer (FRP) reinforcing bars and tendons for concrete, as alternatives to steel reinforcement. The resistance of FRP reinforcement to environmental elements, high strength/weight ratio, and electromagnetic neutrality are among the motivations for this application. There have been many tests on the mechanical behavior of FRP-reinforced concrete to establish the potential of FRP reinforcement in design (see *e.g.*, Nanni (1) and the previous FRPCS Symposia Proceedings), but the analysis of FRP-reinforced concrete has received less attention.

Modeling the behavior of FRP-reinforced concrete requires models for the constitutive behavior of concrete and FRP and a model for their interaction (commonly called *bond*). Reinforcement is often designed to prevent and/or bridge cracks that occur in the concrete. As such, bond behavior is important in determining the nature of localized failures and the amount of energy dissipated by reinforced concrete components. For smooth reinforcing elements, adhesion and friction are the key mechanisms that affect the bond behavior. The frictional behavior is affected by "misfit stresses" (*e.g.*, due to concrete curing) and Poisson's effect. The bond failure in this case consists of the initiation of an interfacial crack, propagation of the crack, and subsequent "frictional smoothing" of the asperities along the crack surface.

This study focuses on the modeling of bond for carbon FRP (CFRP) tendons that have a *significant surface structure* (*e.g.*, ribs). For this case, adhesion breaks down relatively early in the bond response and by design has only a secondary contribution to bond strength. The dominant mechanism for force transfer is the subsequent mechanical interlocking of the reinforcement's surface structure with the adjacent concrete. The importance of this component is demonstrated by the racheting type behavior that has occurred in some pull-out tests subjected to long slips (see *e.g.*, ref. (2)). Under increased monotonic loading the mechanical interlocking can produce: transverse and longitudinal cracking in the concrete, crushing near the contact areas, and shearing with possible mode II cracking in the surface structure of the FRP reinforcement and/or concrete. Combined, these local failures can lead to a progressive bond failure. The contribution of each failure

mechanism depends upon several factors, including the stress state in the damaged region near the interface – the so called *bond zone*. Thus some mechanisms (*e.g.*, transverse cracking) that are important to the bond behavior of steel bars, may be less important for some FRP bars and tendons. Some researchers have partially attributed this difference to the shape and relative compliance of the FRP reinforcement's surface structure.

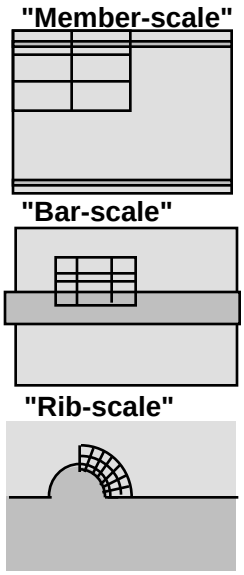

Figure 1. Scales of bond analysis

Bond has been numerically modeled and characterized at several scales. Figure 1 depicts three scales of spatial discretization used in modeling bond (3,4). At a relatively large scale – the *member-scale*, each reinforcing element is treated as a one-dimensional bar element and bond is characterized by a bond stress-slip relationship. The member scale can allow realistic structural problems to be addressed, but this scale also has limitations; *e.g.*, it is too coarse to predict some behaviors such as the propagation of longitudinal cracks to a free surface (which essentially eliminates bond strength). At a much smaller scale – the *rib-scale*, the bar and its surface structure are often explicitly modeled. Rib-scale analyses are very important toward understanding aspects of the underlying mechanics of bond, but generally the simplifying assumptions made limit the models to qualitative evaluations. A scale of compromise – the *bar-scale* – treats the bar and concrete as continua and models the interaction between them without explicitly modeling the surface structure of the bar. This type of model has a phenomenological nature, but potentially it can be used to model the behavior of structural components while including important failure mechanisms such as longitudinal cracking of the concrete adjacent to the bars.

For steel bars, there have been several bond models proposed at each of the above scales, but only a few models have been proposed for FRP bars. As for steel bars, the first bond models for FRP bars have addressed the member scale; see *e.g.*, the models of Faoro (5), Malvar (6), Alunno *et al.* (7), and Cosenza *et al.* (8). Faoro (5), and Alunno *et al.* (7) applied the model of Eligehausen *et al.* (9) which was originally developed for steel bars, and Cosenza *et al.* (8) modified the ascending component of the model. These models relate average bond stress to slip and were derived from curve fits to a single data set. Thus member-scale models generally have two important limitations: (1) they will only predict bond response in structures having a stress history similar to the original specimen, and (2) they can not predict longitudinal cracking in the adjacent concrete. A few rib-scale models have also been proposed. Yonezawa *et al.* (10) presented a rib-scale parameter study apparently idealizing the materials as linear elastic. Boothby *et al.* (11) presented a rib-scale analysis of a bond specimen having an FRP bar with a single rib. The FRP was modeled with an elastoplastic model using a modified Hill criterion, and the concrete was also modeled using an elastoplastic model. Bakis *et al.* (12) adopted a simplified rib-scale model that characterizes the shear behavior of individual ribs with an "elastic-linear softening spring model." The particular bars were designed to fail the ribs in shear.

This study addresses the characterization of bond behavior of FRP tendons at the *bar-scale*. A bond model that was originally developed for steel bars (3,4) was recently applied to the bond of FRP bars (13). The model provides a macroscopic characterization of the bond behavior within the mathematical framework of

elastoplasticity theory. The initial application of the bar-scale model to FRP bars and tendons does not incorporate physical parameters related to constitutive behavior of the FRP, thus we anticipated that the model would have to be recalibrated for reinforcement having "significantly different surface structures." Previous results for FRP bars showed that the bond strength of different specimens could be predicted with acceptable accuracy when the bond model was incorporated into a finite element (FE) model of each specimen. In this paper, we examine the application of the model to predicting the bond strength and transfer length of CFRP tendons.

The next section of this paper presents a brief overview of the elastoplastic bond model with the calibration parameters for a particular FRP bar (13). Section three presents the calibration and validation results, and the last section presents the conclusions.

BOND MODEL

There are several underlying assumptions associated with bar-scale models (4) that for brevity are not discussed here. One common idealization adopted here is that the interaction can be characterized by an interface model where the reinforcing element is modeled as a cylindrical solid. This requires the effects of the mechanical interaction (*e.g.*, the "wedging effect" of the surface structure) to be represented in the interface model formulation. Another assumption is that the interface traction can be homogenized to yield a continuous traction distribution. By not explicitly modeling the surface structure of the reinforcement, the model can be potentially applied to larger scale problems (*e.g.*, to model the progressive failure of a structural component), but it will not provide details on the failure of the mechanical interlocking (*e.g.*, failure of the FRP surface structure versus failure of the adjacent concrete). Another idealization used to simplify the analyses is that the interface behavior can be treated as axisymmetric.

The interface model relates the components of the interface traction to the components of the relative interface displacement. The use of elastoplasticity as a mathematical framework for the model was originally motivated by the classical elastoplastic behavior of many early bond specimens (see *e.g.*, ref. (9)). The model is defined by the generalized stresses and strains, internal variables, yield criterion, elastic moduli, and flow rule.

The generalized stresses (**Q**) are the tangent and normal components of the interface traction, τ and σ respectively. τ is referred to as the *bond stress*, and $-\sigma$ will be referred to as the *confinement stress*. (σ is positive in tension.) The generalized strains (**q**) are defined as the tangent (δ_t) and normal (δ_n) displacements of the concrete surface measured relative to the bar surface and nondimensionalized by the bar diameter (D_b); *i.e.*, $\mathbf{q}^T = (\delta_t/D_b,\ \delta_n/D_b)$. For monotonic loading, the evolutions of the yield surface and flow rule are characterized by a single measure of the internal state, the bond zone "damage" which is defined as

$$d = \min\left(\left|\delta_t^p\right|/s_r, 1\right) \tag{1}$$

where δ_t^p is the plastic slip and s_r is a characteristic length of the surface structure (*e.g.*, the rib spacing). The terminology "damage" indicates that d is a measure of

the physical damage at the rib-scale.

For the application to FRP reinforcement the yield criterion is of the form $f(\tau, \sigma, d) = 0$ with

$$f(\tau,\sigma,d) = \frac{|\tau|}{f_t} - C(d)\left|\hat{\sigma}(d) - \frac{\sigma}{f_t}\right|^{\alpha_p} \quad (2)$$

where: f_t ~ tensile strength of concrete; C ~ isotropic hardening/softening function; $\hat{\sigma}$ ~ kinematic softening function; α_p ~ a model parameter with a calibration value of 0.75.

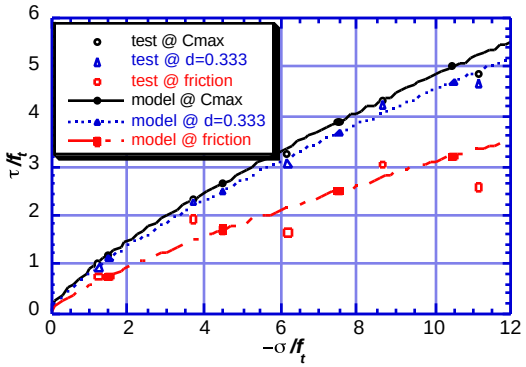

Figure 2. Yield surface *vs*. exp. data.

The calibration of the model for this study was obtained via simplified analyses of the experimental results of Malvar (6) for his "type d" GFRP bars; additional details on the calibration (including some discussion on the effects and physical meaning of selected model parameters) are given in ref. (13). We originally anticipated that the model would only reproduce experimental results accurately when the calibration and validation specimens had "similar concrete strengths" and bars with "similar surface structures." However the range of applicability of a given calibration is not known.

The Malvar experiments are useful for formulating and calibrating phenomenological models because they provide data at different stress states. (Some data for the specimen are given in Table 1.) The FRP bar is centered in a small concrete cylinder that is cast inside of a slotted pipe. The pipe is later enclosed in a circumferential band that has two purposes: (1) to apply uniform normal tractions to the outer surface of the specimen and (2) to measure the change in circumference which is then used to calculate the radial dilation of the interface. The slotted pipe apparatus is loaded under displacement control, while a hydraulic clamp is used to apply constant confining pressure. Malvar's tests were conducted in sets of five: one specimen at each confinement pressure (500, 1500, 2500, 3500, and 4500 psi; *i.e.*, 3.45, 10.3, 17.2, 24.1, and 31.0 MPa). The reported confinement pressures are the average values of $-\sigma$ that would occur if the concrete did not carry hoop stress. To "uncouple" the bond behavior from the concrete splitting response the specimens were "pre-loaded" to split the concrete prior to performing the bond tests. The disadvantage to this approach is that the initial extent of damage in the bar surface structure and concrete was unknown.

Figure 2 shows how the yield surface model fits the experimental data for a few given states of interface damage. Additional details of the calibration procedure and physical interpretation of model parameters are given in ref. (4). For small values of d, C initially opens the surface (the hardening phase) and then subsequently closes the surface (the softening phase) representing the progressive failure of the mechanical interlocking. $\hat{\sigma}$ rapidly translates the yield surface to the origin of the stress-space, which for some reinforcement partially characterizes the change in contact conditions at low confinement stresses.

The strains are additively decomposed into elastic ($\mathbf{q}^e$) and plastic ($\mathbf{q}^p$) components. The relationship between stresses ($\mathbf{Q}$) and elastic strains ($\mathbf{q}^e$) is assumed to have the linear form: $\mathbf{Q} = \mathbf{D}^e \mathbf{q}^e$ where the elastic moduli are defined as

$$\mathbf{D}^e = \begin{bmatrix} E_c / k_0 & 0 \\ 0 & E_c / (k_1 + k_2 q_2^p) \end{bmatrix} \tag{3}$$

E_c is Young's modulus of the concrete, and k_0, k_1, and k_2 are model parameters. k_0 is obtained by calibrating the model to accurately represent the initial elastic bond stress-slip response. k_1 and k_2 define the radial elastic response, which is very important in the prediction of longitudinal cracking. When k_2 is nonzero, the elastic response depends upon the plastic dilation (elastoplastic coupling). This aspect of the model is defined to characterize the effect of changing contact conditions along the interface upon the effective elastic modulus associated with the interface. Closed form analytical results for an idealized case that show how the effective elastic modulus changes with traction distribution are given in ref. (14). The calibrated parameters used in this study are: k_0 = 10, k_1 = 0.034, and k_2 = 27.

The kinematic effects of the wedging action between the bar's surface structure and the adjacent concrete is accounted for in the bar-scale model by the flow rule. The flow rule determines the extent of radial dilation at the interface which produces hoop stress in the adjacent concrete. The adopted form of the flow rule is given by

$$\dot{\mathbf{q}}^p = \dot{\lambda} \begin{bmatrix} \text{sgn}(\tau) \\ g(\sigma, d) \end{bmatrix} \tag{4}$$

where $\dot{\lambda}$ denotes the consistency parameter. To obtain an approximation for g, limited data presenting radial dilation versus slip (6) were analyzed. As with the yield surface evolution, g is assumed to be only dependent upon $-\sigma$ and d. The model approximation of g is shown in Figure 3. The function g quantifies the rate of plastic radial dilation with respect to plastic slip. Therefore the area under each curve in Figure 3 is proportional to the maximum radial dilation that would occur for a constant value of σ. These data reflect a key behavior that a model of this type must quantify to predict both the bond stress-slip behavior and potential splitting failures: radial dilation decreases with an increase in the confinement stress.

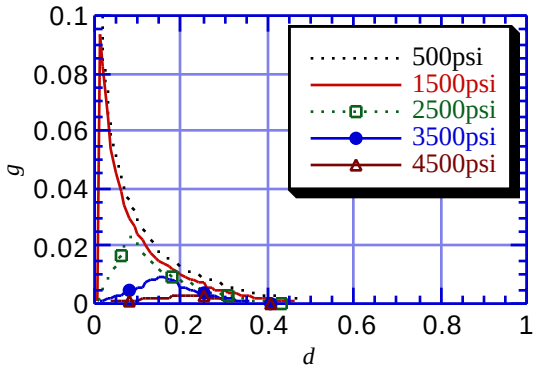

Figure 3. Flow rule

The coupling of the longitudinal and radial responses both in terms of the progressive failure and kinematics distinguishes this approach from member scale models because this type of model: (1) actively contributes to the stress state near the bar through the radial dilation and thus can produce longitudinal cracking in the adjacent concrete; and (2) stress state dependency of the model can potentially allow the model to be applied to a wider range of specimens without recalibration.

CALIBRATION AND VALIDATION RESULTS

This section presents calibration and validation results for the model. The emphasis of this paper is upon applying the model to predict the bond strength and transfer lengths of CFRP tendons. To validate the model over a wide range of tests a CFRP

tendon was selected for which several experimental studies are reported in the literature – the CFCC (carbon fiber composite cable) developed by the Tokyo Rope and Toho Rayon companies. This tendon consists of seven CFRP rods, six of which are helically wrapped around a central rod. Each individual rod consists of carbon fibers in an epoxy matrix wrapped within a protective carbon fiber covering.

Two general types of validation problems are considered: pull-out tests and transfer length tests, with the emphasis on the former. Some general data for the calibration and validation specimens are presented in Table 1. Note in particular that for the pull-out tests there is a wide variation in specimen attributes: the embedment (or bond) lengths vary from about $3D_b$ to about $14D_b$, the bar diameters vary by a factor of about 2.5, and the concrete strengths vary by a factor of about 2.

An inherent difficulty in characterizing bond behavior is that it can not be experimentally isolated; it is integrally tied to the bond specimen, since it is a structural response. Thus, to simulate the response of a given test requires a model of the bond specimen. The specimens were modeled using axisymmetric finite elements. For the transfer length specimen the diameter was defined so that the cross-sectional area of the concrete remained the same as the square section.

The concrete was modeled as an isotropic elastic material until the hoop stress reached the tensile strength. When the concrete tensile strength was unknown, it was estimated by the empirical relationship $f_t = 0.3 f_{cK}^{2/3}$ MPa, where f_{cK} is the characteristic compressive strength in MPa (see ref. (17)). Longitudinal cracks were incorporated into the models by adopting a "smeared crack" approach in the hoop direction; *i.e.*, the effective strain in the hoop direction was the sum of the strain in the bulk material and the smeared effect of the opening of longitudinal cracks. The number of longitudinal cracks was pre-defined, and these cracks were assumed to evolve concurrently separating the concrete in the cracked region into equal size sectors. This axisymmetric idealization to incorporate the effects of longitudinal cracking in the FE modeling follows the approach of Rots (18). Each crack is idealized as being planar with a process zone of infinitesimal thickness and finite length. The process zone in the plane of the crack (commonly referred to as the *cohesive crack* (20)) represents the effects of crack bridging by the aggregates. The behavior of the process zone is characterized by the following traction–crack opening relationship: $\sigma_{cr} = f_t(1.0 - \hat{w}^k)$ where $\hat{w}$ is the ratio of the opening displacement of the cohesive crack and the critical crack opening (*i.e.*, the minimum

Table 1. Test specimen data for CFCC tendons.

Experiments	Specimen Size ($L\times D$ *or* $L\times W\times H$) (mm)	Bar Diameter D_b (mm)	Bond Length L_b (mm)	Concrete Strength f_c (MPa)
Calibration test				
Malvar (6)	102×76	19	66.7	29.1
Validation pull-out tests				
Tepfers *et al.* (15)	48×114	12.5	48	47.3
Tepfers *et al.* (15)	200×200×200	12.5	45	44.4
Tokyo Rope (16)	150×100×100	12.5	150	47.6
Benmokrane & Chennouf (2)	150×57	7.3	100	61.6
Validation transfer length test				
Tepfers *et al.* (15)	2000×70×70	12.5	2000	39.4

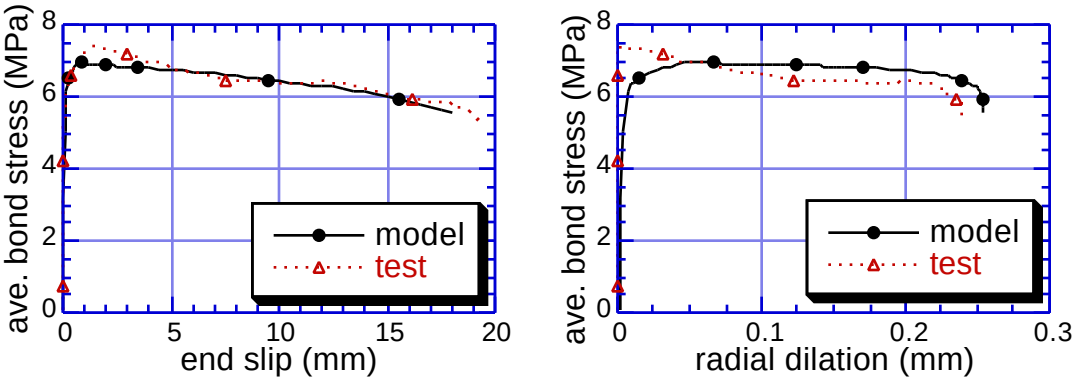

Figure 5. Bond model calibration results for σ=–1500 psi (10.3 MPa).

crack opening, w_o, for which there is no traction across the crack), f_t is the tensile strength of the concrete, and k is a model parameter. For the validation problems presented here, k = 0.248 and w_o is selected so that the model reproduces the estimated *fracture energy*. The fracture energy and Young's modulus for most concrete specimens was estimated from the empirical relations given in CEB (17).

The CFCC tendon was idealized as a transversely isotropic solid with the elastic constants estimated using the approximate formula of Hashin (1983).

Calibration Results

The calibration is based upon the experimental data of Malvar (5) for a GFRP bar that has a helical indentation (type d). They are significantly different than the CFCC tendons considered in this study, so initially these calibration results were not anticipated to be adequate for predicting the bond behavior of the CFCC tendons. However, experimental data for the CFCC tendons that address the bond response dependency upon the stress state in the concrete are not yet available, so these calibration data were considered to be a first estimate of the bond behavior that would need refinement. The validation results that follow show that the model gives acceptable predictions without additional refinement of the calibration.

One of the calibration results is shown in Figure 5. This particular calibration result (see Table 2) is for σ = –1500 psi. The radial dilation for these tests indicates the tendency for the mechanical interlocking to produce longitudinal cracking. The magnitudes of the radial dilation at various levels of confinement stress are very similar to the experimental values observed for steel bars of the same diameter (21). For σ = –1500 psi the radial dilation for a steel bar was 0.22 mm.

Validation Results

Most of the validation tests considered are pull-out tests. Comparisons of experimental and numerically predicted bond strengths are shown in Table 2. The model is also used to predict the transfer length for a particular test.

Table 2. Validation results for CFCC tendon pull-out tests.

Experiments	Specimen Size ($D\times L$ *or* $L\times W\times H$) (mm)	Concrete Strength f_c (MPa)	Maximum Bond Stress (MPa)		
			Test	Model	Difference
Calibration test					
Malvar (6)	102×76	29.1			
500 psi			3.83	4.19	9 %
1500 psi			7.40	6.68	10 %
2500 psi			10.42	9.37	10 %
3500 psi			12.07	11.95	1 %
4500 psi			13.47	14.38	7 %
Validation tests					
Tepfers *et al.* (15)	48×114	47.3	9.46	9.20	3 %
Tepfers *et al.* (15)	200×200×200	44.4			
min @ slip 0.6 mm			10.5		
max @ slip 0.6 mm			12.7		
avg @ slip 0.6 mm			11.6	10.6	9 %
Tokyo Rope (16)	150×100×100	47.6			
monotonic loading			7.22	6.51	10 %
cyclic-mono. loading			6.86	6.51	5 %
Benmokrane & Chennouf (2)	150×57	61.6	10.8	12.6	16 %

The first validation test considered is the "ring test" of Tepfers *et al.* (15). For these tests the concrete is cast within a steel ring that is strain gauged to measure the hoop strain. The hoop strain provides a measure of the "splitting tendency of each tendon." Figure 6 shows a FEM model of the specimen (which is representative of those used in this study).

Figure 7 shows the comparison of the experimental data and model predictions. The agreement between the two responses is excellent. While the extent of experimental scatter that would occur with multiple tests is unknown, previous ring tests for steel bars exhibited relatively little scatter. It appears that both the initial stiffness and bond strength would be predicted

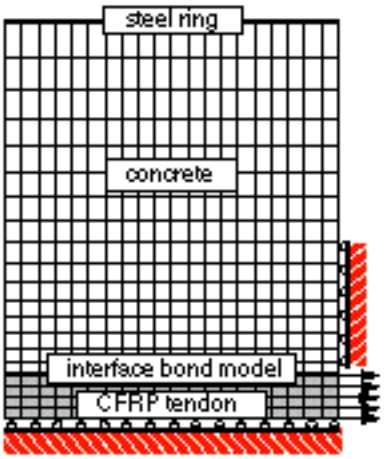

Figure 6. Specimen model of the Tepfer *et al.* ring test.

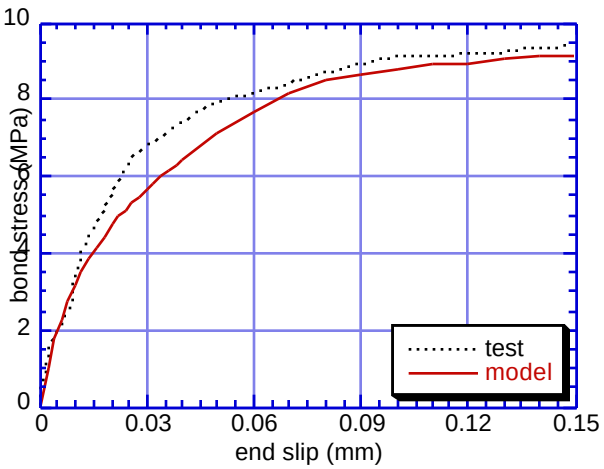

Figure 7. Tepfers *et al.* ring test: exp. *vs*. model.

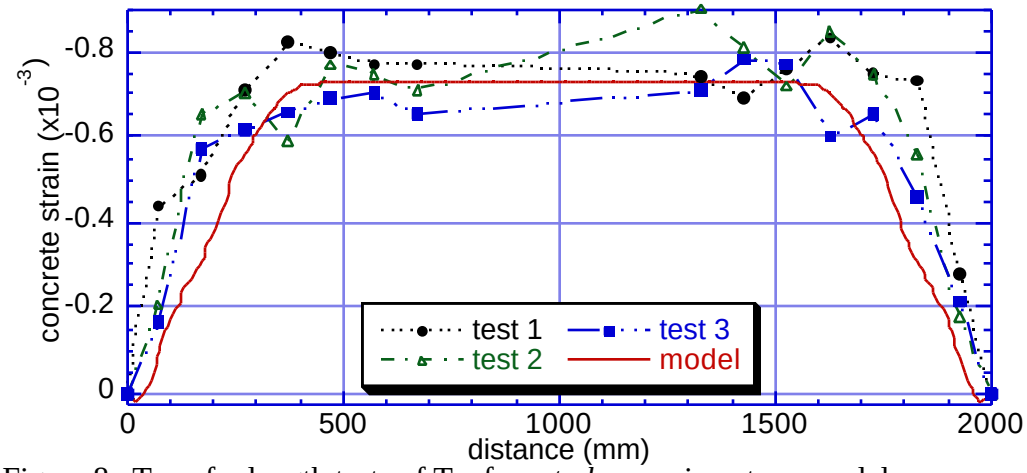

Figure 8. Transfer length tests of Tepfers *et al.*: experiment *vs*. model.

accurately. The maximum bond stress is not provided, so the comparison shown in Table 2 applies to the bond stress at a slip of 0.15 mm.

The second pull-out test considered is also presented by Tepfers *et al.*. This specimen is cubic in shape. The bond strength and initial stiffness (though not shown here) are again predicted with acceptable accuracy. The bond strength is predicted within about 9 percent of the "average value."

The third pull-out test is based upon data provided by the Tokyo Rope Manufacturing Company (16). The specimen diameter for the model was 100 mm. Two experimental results are given: one for the case of simple monotonic loading, and the second for a monotonic test that occurred after ten load cycles to a tendon force of 34.3 kN. The bond model presented here is only applicable to monotonic loading, but the comparison to both experimental values (Table 2) is shown to be of acceptable accuracy.

The last pull-out test addresses a study by Benmokrane and Chennouf (2) for examining the behavior of cement grouted anchors. The experimental result shown here is for a CFCC tendon with a nominal diameter of 7.5 mm. The grout was a plain grout (CG1) made from ASTM Type I Portland cement. The grout was cast within a 57 mm inner diameter steel tube with a wall thickness of 3 mm. Table 2 shows that the model over-estimated the maximum bond strength of the experiment by about 16 percent.

Lastly, a transfer length test by Tepfers *et al.* (15) is considered to further demonstrate the predictive capabilities of the model. Unlike the pull-out tests Poisson's effect will increase $-\sigma$ at the interface, an effect that the stress state dependency of the bond model can potentially account for. The CFCC is prestressed to 59 percent of the ultimate load. The axial strain in the concrete was measured on two opposite faces of the square cross section, on 100 mm intervals from the ends (to 700 mm from each end). In modeling the specimen, symmetry is assumed and thus only half of the specimen was modeled. The test was modeled by initially prescribing the bar loads and a uniaxial prestress in the bar. Under successive load steps the traction at the end of the bar is reduced to zero. Based upon the measured strain, Young's modulus for the concrete was estimated to be 20,375 MPa. Figure 8 shows the simulation and test results. The transfer length in these tests was defined as the distance from the end at which the full prestress force

was "transferred into the concrete." The model predicts that this occurs between 400 to 500 mm from the end. A nominal value of 450 mm differs from the experimental estimate (400 mm) by about 13 percent.

CONCLUSIONS

The objective of coupling the characterization of longitudinal and radial bond behavior with an elastoplastic model was to develop a model that had a measure of generality. The phenomenological nature of the model will generally require it to be recalibrated for "significantly different" FRP bars and tendons; however, using a previous calibration for a GFRP bar, the model gives acceptable estimates of the bond strength for several tests of CFCC tendons even though the specimens have significantly different attributes. Additional validation problems are needed to define the predictive limits of the model. Nonetheless, the transfer length problem further demonstrates the potential application of the model to help predict and understand the behavior of FRP-reinforced structural components.

ACKNOWLEDGMENTS

Support for this study by the National Science Foundation (grant no. CMS-9872609) and the Naval Facilities Engineering Service Center (contract no. N0024498P0366) are gratefully acknowledged.

REFERENCES

1. Nanni, A. ed. (1993). Fiber-reinforced- plastic (FRP) reinforcement for concrete structures: Properties and applications, Elsevier Science Publisher.

2. Benmokrane, B. and A. Chennouf (1997). "Pull-out behavior of FRP ground anchors," *Proceedings of the 42nd International SAMPE Symposium and Exhibition*, Anaheim, CA, vol. 42, no. 1, pp. 311-324.

3. Cox, J.V. and Herrmann, L.R. (1992). "Confinement Stress Dependent Bond Behavior, Part II: A Two Degree of Freedom Plasticity Model," *Bond in Concrete, Proc. of the Int. Conf.*, CEB, pp. 11.11-11.20.

4. Cox, J.V. and L.R. Herrmann (1998). "Development of a plasticity bond model for reinforced concrete," *Mech. of Cohesive-Frictional Mat.*, vol. 3, pp. 155-180.

5. Faoro, M. (1992). "Bearing and deformation behavior of structural components with reinforcements comprising resin glass fiber bars and conventional ribbed steel bars," *Bond in Concrete, Proc. of the Int. Conf.*, CEB, pp. 8.17-8.26.

6. Malvar, L.J. (1995). "Tensile and bond properties of GFRP reinforcing bars," *ACI Materials Journal*, vol. 92, no. 3, pp. 276-285.

7. Alunno, R. V., D. Galeota, and M. M. Giammatteo (1995). "Local bond stress-slip relationships of glass fiber reinforced plastic bars embedded in concrete," *Materials and Structures*, vol. 28, no. 180.

8. Cosenza, E., G. Manfredi, and R. Realfonzo (1995). "Analytical modeling of bond between FRP reinforcing bars and concrete," *Non-metallic (FRP) Reinforcement for Concrete Structures*, L. Taerwe ed., pp. 164-171.

9. Eligehausen, R., E. P. Popov, and V. V. Bertero (1983). "Local bond stress-slip relations of deformed bars under generalized excitations," *Report UCB/EERC-83/23*, University of California, Berkeley, CA.

10. Yonezawa, T., S. Ohno, T. Kakizawa, K. Inoue, T. Fukata, and R. Okamoto (1993). "A new three-dimensional FRP reinforcement," in *Fiber-Reinforced-Plastic (FRP) for Concrete Structures: Properties and Applications*, A. Nanni ed., Elsevier Science Publishers, pp. 405-418.

11. Boothby, T.E., A. Nanni, C. Bakis, and H. Huang (1995). "Bond of FRP Rods Embedded in Concrete," *Proceedings of the 10th ASCE Engineering Mechanics Specialty Conference*, May, pp. 114-117.

12. Bakis, C.E., V.S. Uppuluri, A. Nanni, and T.E. Boothby (1998). "Analysis of bonding mechanisms of smooth and lugged FRP rods embedded in concrete," *Composites Science and Technology*, vol. 58, pp. 1307-1319.

13. Guo, J. and J.V. Cox (1998). "An Interface Model for the Mechanical Interaction between FRP Bars and Concrete," accepted for publication, *Journal of Reinforced Plastics and Composites*.

14. Cox, J.V. and H. Yu (1998). "A micromechanical analysis of the radial elastic response associated with slender reinforcing elements within a matrix," accepted for publication, *Journal of Composite Materials*.

15. Tepfers, R., I. Molander, and K. Thalenius (1992). "Experience from testing of concrete reinforced with carbon fiber and aramid fiber strands," *XIV. Nordic Concrete Cong. & Nordic concrete Ind. Mtg*, Aug., pp. 337~347

16. Tokyo Rope Mfg Co. Ltd. (1989). "CFCC technical data," *Corporate Report.*

17. CEB (1993). "CEB-FIP model code 90," Redwood Books, Trowbridge, Wiltshire, U.K.

18. Rots, J.G. (1988). *Computational Modeling of Concrete Fracture*, Ph.D. dissertation, Delft University of Technology, Delft.

19. Hillerborg, A., M. Modéer, and P.A. Petersson (1976). "Analysis of crack formation and crack growth in concrete by means of fracture mechanics and finite elements," *Cement and Concrete Research*, vol. 6, pp. 773-782.

20. Hashin, Z. (1983). "Analysis of composite materials - A Survey," *Journal of Applied Mechanics*, vol. 50, pp. 481-505.

21. Malvar, L.J. (1992). "Bond of Reinforcement under Controlled Confinement," *ACI Materials Journal*, vol. 89, no. 6, pp. 593-601.